Journal Name

ARTICLE TYPE

Cite this: DOI: 10.1039/xxxxxxxxxx

The Impact of Viscoplastic Drops on a Heated Surface in the Leidenfrost Regime

Simeng Chen* and Volfango Bertola*

Received Date
Accepted Date

DOI: 10.1039/xxxxxxxxxx

www.rsc.org/journalname

The impact morphology of viscoplastic drops on a heated surface in the Leidenfrost regime is investigated experimentally by high-speed imaging. In particular several important parameters which characterize the impact morphology (such as maximum spreading diameter, minimum retracting diameter and maximum bouncing height etc.) are measured by analysing the impact process, recorded using a high-speed camera. It is shown that as the yield stress grows, surface forces are no longer able to minimize the free surface of the drop, and the inertial deformation upon impact becomes permanent. For small values of the yield stress, the impact morphology of viscoplastic Leidenfrost drops is similar to that of Newtonian drops. These effects can be interpreted in terms of the Bingham-Capillary number, which compares the yield stress magnitude and the capillary (Laplace) pressure. These results suggest that the main contribution to drop rebound is due to surface forces, and not to the intrinsic elasticity of the vapour cushion between the drop and the surface, which is a major assumption in one of the existing models.

1 Introduction

When a liquid droplet impacts on a high-temperature surface, one may observe bouncing back of the droplet off the surface due to the creation of a thin vapour film between the drop and surface upon impact. This is known as 'dynamic Leidenfrost phenomenon'[1–4], and in some sense it is analogous to drop levitation on an air cushion[5,6]. The morphology of this phenomenon is relatively simple. After impact, the drop spreads inertially over the vapor film in a short time (about 5 ms), until it reaches maximum spreading. Then two different outcomes are possible depending on the impact velocity, the fluid properties, and the surface temperature; for high impact kinetic energies, the drop will disintegrate into smaller droplets (splashing); Otherwise, it will recoil under the action of surface forces, to minimize the surface energy, and eventually bounce off the surface if there is sufficient kinetic energy at the end of the recoil. Rebound is eased by the vapour film, which acts as a lubricant layer, reducing frictional energy dissipation both during the initial inertial spreading of the drop and the following recoil. Since the liquid is not in contact with the surface, bouncing Leidenfrost drops represents a unique model system to investigate the dynamics of drop impact independently of wetting and contact angle hysteresis. The rebound of liquid drops on heated surfaces in the Leidenfrost regime was extensively studied for simple Newtonian fluids, in particular water and hydrocarbon liquid fuels[7–11].

Whilst the study of Newtonian Leidenfrost drops dates back to several decades, the advancement of technology enabled a renewed interest in the experimental investigation of this subject in recent years[4,10]. However, it must be remarked that one of the recent works[12] appears to be inconsistent with the previous literature, probably due to a flaw in the experimental procedure[13+].

Although the fluids used in most applications are Newtonian, the interest for non-Newtonian liquids is rapidly growing. Recently, the dynamic Leidenfrost phenomenon was investigated for a range of dilute polymer solutions, which exhibit shear-thinning and/or viscoelastic behaviors[14–18]. The objective of this work is to extend the study of the Leidenfrost drop impact process to a particular type of non-Newtonian fluids, known as viscoplastic or yield-stress fluids. In this case, the Leidenfrost drop impact represents a model system to investigate the behaviour of a viscoplastic fluid where the yield stress is of the same order of magnitude as the Laplace pressure.

Viscoplastic fluids are an important type of non-Newtonian soft materials, which respond like elastic solids for applied stresses lower than a certain threshold value, called yield stress, and flow only when the yield stress is overcome. Practically, this behavior describes many situations, including slurries and suspensions, some polymer solutions, crystallizing lavas, muds and clays, heavy oils, avalanches, cosmetic creams, hair gel, liquid chocolate, and some pastes. Consequently, yield stress fluids have

* *Laboratory of Technical Physics, School of Engineering, University of Liverpool, The Quadrangle, Brownlow Hill L69 3GH, United Kingdom. E-mail: Volfango.Bertola@liverpool.ac.uk*

+ *This paragraph was added on explicit request of an anonymous Referee.*

applications in many different fields, ranging from the oil, gas and chemical industries, to food processing, cosmetics and geophysical fluid dynamics. This unique property can affect both the process of the formation of a drop from a capillary nozzle[19] and the interactions between yield-stress drops and solid surfaces[20,21]. A recent study of yield-stress drops impacting on pre-coated surfaces showed that the presence of yield stress enables drops to stick to a surface, inhibit splash, and form a lump or crater[22]. Also in contrast to impacts on dry surfaces, the formation of large long-lifetime ejection sheets with redirected momentum which extend away from the impact location was observed for pre-coated surfaces. The spreading of axisymmetric viscoplastic droplets extruded slowly on glass surfaces was investigated experimentally using shadowgraphy and swept-field confocal microscopy[23]. In this study, the confocal microscopy system enables one to directly measure the vertical profile of the radial velocity, revealing apparent slip of spreading drops of viscoplastic fluids (Carbopol solutions) over untreated glass surfaces, which is a factor that has not always been considered explicitly.

In principle, the rebound of Leidenfrost drops results from the combination of two independent mechanisms: (i) the rapid release of the surface energy stored during inertial spreading, and (ii) the elasticity of the compressible vapor film between the drop and the surface[1]. The former mechanism is also responsible for drop rebound on non-heated, hydrophobic surfaces (where no vapour film exists)[24,25]. After inertial spreading, the drop tends to recover its spherical shape in order to minimise its surface energy, therefore the excess surface energy stored during spreading is converted into kinetic energy, and propels the drop off the surface, as illustrated in Figure 1a. In several Leidenfrost drop models, rebound is described using only the surface energy approach, while the elasticity of the vapor layer is not considered explicitly. The only effect of the vapor layer is to introduce a slip boundary condition at the liquid-solid interface. The good agreement between numerical results and experimental data indicates that Leidenfrost drop rebounds can be explained by the surface tension mechanism alone[26,27].

However, some authors suggest the rebound is also due to the formation of a high-pressure vapor layer between the liquid and solid surface during impact. The high-pressure vapor layer is working as an elastic cushion which provides forces opposite to the impact velocity. The upward forces cause a change in the momentum of impinging drop leading to its reflection, as shown schematically in Figure 1b. In the so-called disk model[1], rebound is driven by the cushion mechanism, in which the shape dynamics of the liquid drop is not considered (i.e. radius and thickness of the liquid disk are constant).

The special property of yield-stress fluid enables one to examine the two reflection mechanisms by conducting Leidenfrost drop impacts using viscoplatic drops with different magnitudes of yield stress. At the end of spreading the liquid lamella is static (i.e. there is no inertial force). Hence the retraction is a result of the competition between the driving surface tension forces and the resisting yield-stress forces, which can be expressed as the Bingham-Capillary number, $B = \tau_0 D_0/\sigma$, where τ_0 is the yield stress and σ the surface tension[28]. At high Bingham-Capillary numbers ($B > 1$) the surface tension can no longer overcome the yield-stress causing only little retraction compared with low B cases, resulting in an oblate shape of a bouncing drop. Through the comparisons of the maximum bouncing height of yield-stress drops with different Bingham-Capillary numbers at the same impact Weber number, the contribution of the elastic vapor cushion to the reflection can be evaluated, which will be discussed in section 3.

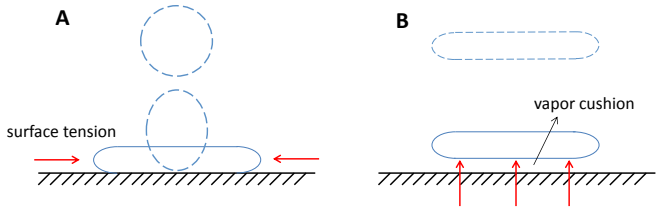

Fig. 1 Rebound mechanisms of a drop impinging on a hot surface: (A) surface tension; (B) vapor cushion.

2 Experimental method

Viscoplatic fluids were prepared by dispersing Carbopol 940 powder (Lubrizol, $\rho = 1400$ kg/m^3) into de-ionised water (Barnstead Easypure); aqueous NaOH solution (30% w/w) was then used to neutralise the Carbopol dispersions[29,30]. Fluids with six different concentrations of Carbopol (Ca 0.067%, 0.079%, 0.1%, 0.113%, 0.124% and 0.142% w/w, respectively) were prepared in order to study the effect of large variations of the yield stress on drop impact behaviour. Viscosities of the model viscoplastic fluids were measured using a rotational rheometer (TA Instruments AR 1000) with a parallel plate geometry (diameter: 40 mm) with rough surfaces to avoid wall slip artefacts. The measured flow curves are shown in Figure 2a; to identify the yield stress, viscosity data obtained for shear stresses above the yield point were fitted with the Herschel-Bulkley (H-B) model, as shown in Figure 2b:

$$\tau = \tau_0 + k\dot{\gamma}^n. \quad (1)$$

where τ is the shear stress, τ_0 the yield stress, $\dot{\gamma}$ the shear rate, k the consistency index, and n the flow index. The resulting yield stress values for Carbopol solutions of different concentrations were shown in Table 1, which is consistent with values reported in the reference literature[30]. The concentrations of the Carbopol solutions were intentionally selected to yield a Bingham-Capillary number range covering unity, which enabled the yield stress to suppress the retracting forces from surface tension at relatively high B numbers.

Table 1 Properties of model viscoplastic fluids

Ca	0.067%	0.079%	0.1%	0.113%	0.124%	0.142%
Yield stress (Pa)	1.13	3.64	11.7	21.1	29.1	56.5
Surface tension (mN/m)	66	66	66	66	66	66
Density ($\times 10^3$ kg/m^3)	1	1	1	1	1	1
Equilibrium drop diameter (mm)	3.04±0.08	2.99±0.04	2.96±0.12	2.74±0.06	2.67±0.06	2.64±0.05
Bingham-Capillary $B = \tau_0 D_0/\gamma$ (-)	0.052	0.16	0.52	0.88	1.2	2.3

An estimate of the heat transfer between the drop and the surface suggests that, even for drop diameters of few millimetres, and in the most favourable heating conditions, the average temperature of the drop increases by only about 10°C with respect to the ambient temperature[18]. Thus, one can evaluate the fluid properties at ambient temperature as a first approximation.

The experimental setup is schematically described in Figure 3. Drops were released from a blunt hypodermic needle (gauge 21, i.d. 0.495 mm) and impacted on a polished aluminium surface, kept at the temperature of 400°C. Temperature could be controlled within ±1°C by a PID controller driven by a K-thermocouple placed 1 mm below the point of impact. This temperature is high enough to keep the vapour film stable and avoid the formation of secondary droplets[1,8,15,16]. Drop weight measurements made with a precision balance (Mettler PM 100) allowed calculation of the drop diameter at equilibrium, $D_0 = \sqrt[3]{(6m/\pi\rho)}$. Values of equilibrium drop diameters were obtained from averages over 50 samples as shown in Table 1. Adjusting the position of the dispensing needle with a digital height gauge allowed one to change the impact velocity hence the impact Weber number, $We = \rho D_0 u_i^2/\sigma$, which expresses the competition between kinetic energy and surface energy. The impact velocities u_i were measured through digital image processing, with accuracies ranging between a minimum of 2 mm/s and a maximum of 20 mm/s. A systematic investigation on the measurements of the surface tension of viscoplatic fluids by Boujlel et al. showed that Carbopol gels appear to have almost the same value (0.066 N/m) of surface tension whatever their yield stress, but this value is almost 10% smaller than that of pure water at ambient temperature: 23°C[31]. This value of the surface tension of Carbopol gels is applied in the calculation of Weber number in the present work since our experiments were conducted at a close ambient temperature: 20°C. For each set of experimental parameters (i.e., polymer concentration and Weber number), the impact experiment was repeated five times for the sake of statistical analysis.

The impacts of single drops were recorded using a high-speed CMOS camera (Mikrotron MC1310) at the rate of 1000 frames per second and a resolution of 560x514 pixels, which allowed measurements with a typical resolution of 27 μm/pixel. The camera was horizontally aligned with the impact surface in order to measure the bouncing height of the drop with precision. Back-to-front illumination was provided by an LED lamp (Philips Accent LED), which ensured a uniform intensity in the field of view. Drop impact movies were analysed using a custom-built LabView application operating in two stages: in the first, the background is subtracted from each frame and the image brightness, contrast, gamma correction, and digital gain can be adjusted manually; in the second stage, the application extracts from each frame, the gap between the drop and the surface, G, and the horizontal and vertical dimensions of the drop, D_h and D_v , normalized with respect to the equilibrium drop diameter. From these measurements, the height of the drop center of mass was calculated as $H = G + D_v/2$ (note that such definition relies on the assumption drops are symmetric during rebound, which is not always the case).

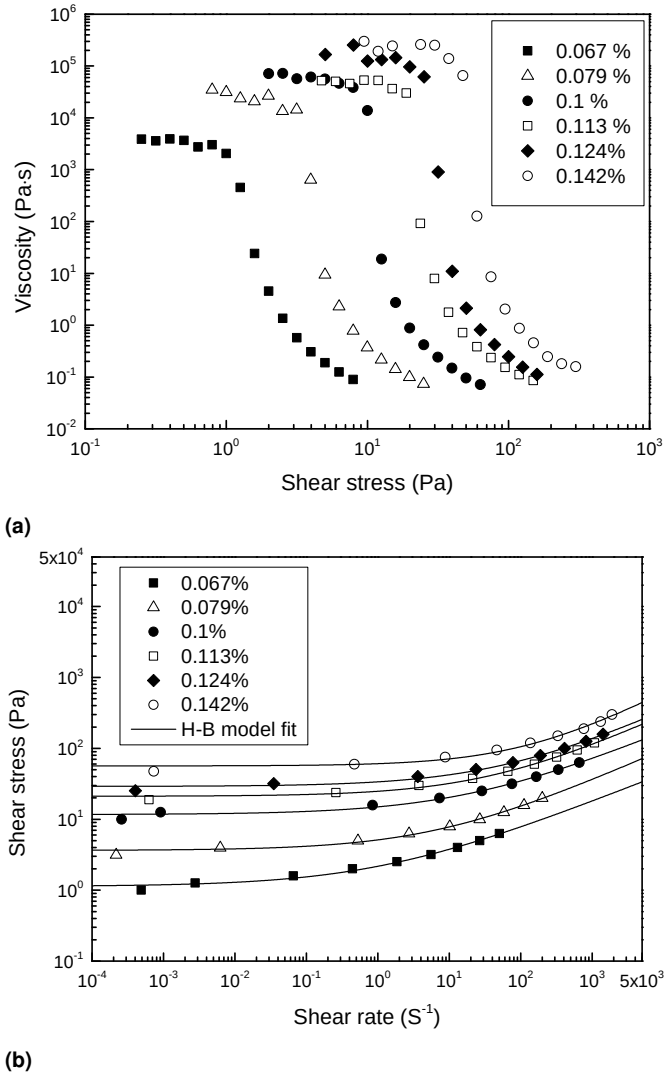

Fig. 2 (a) Flow curves of the model viscoplatic fluids of different concentrations; (b) Shear stresses of the model fluids as a function of shear rates and the corresponding H-B fit curve.

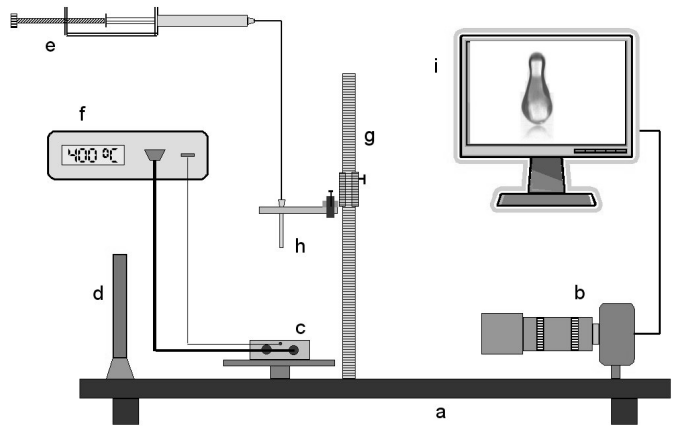

Fig. 3 Schematic of the experimental setup: (a) optical breadboard; (b) high-speed camera; (c) heated aluminium block; (d) LED backlight; (e) drop dispensing system; (f) temperature controller; (g) height gauge; (h) needle; (i) computer.

3 Results and Discussion

3.1 Morphology

The impact morphology of different viscoplastic Leidenfrost drops at low impact Weber number (10∼20) and high impact Weber number (100∼120) are shown respectively in Figure 4a and Figure 4b. Specifically four important moments during the whole impact process are selected: beginning of impact, maximum spreading, beginning of bouncing and maximum bouncing. The shape of viscoplastic drop produced from a capillary nozzle becomes more prolate when B increases (Figure 4a) since the surface tension is not able to deform the natural prolate shape forming under the needle due to the existence of high yield-stress[19]. This effect weakens at high impact Weber number, due to a longer falling time for drops to reach spherical shape at higher releasing position (i.e. higher Weber). It is obvious that the spreading is inhibited for drops with high values of B: at low We drops with high B ($B = 1.2$ & 2.3) end up with a conical shape during spreading while others form a disk-like shape; at high We drop with higher B tend to achieve a thicker liquid lamella with shorter radius. This is associated with high viscous energy dissipation in drops with a high value of yield-stress. Retracting behaviors of low B drops are much more pronounced as revealed by the long prolate shapes at the beginning of bouncing. They also bounce higher compared with high B drops. In the middle range of B (0.16∼1.2), there is a monotonous decrease in the maximum bouncing height with respect to the B number.

3.2 Maximum spreading diameter

The diameter of the lamella formed at the end of the spreading stage is called the 'maximum spreading diameter' (D_{max}). The value of this parameter is proportional to the surface energy of the drop at the end of spreading hence it is also an indicator of the energy dissipation during the spreading process if the initial kinetic energy (i.e. the We) of the drop remains unchanged[17]. Figure 5 shows the normalised maximum spreading diameter with respect to the equilibrium drop diameter (D_{max}/D_0) of the drops of model fluids as a function of the impact Weber number. The maximum spreading diameter decreases monotonously with respect to B number since larger B number means more viscous energy dissipation during spreading. For each model viscoplastic drop (i.e. the same B), the correlation between D_{max}/D_0 and We follows the scaling law: $D_{max}/D_0 \sim We^{\alpha}$ [9]. The experimental data of the most concentrated solution ($B = 2.3$) and the least ($B = 0.052$) are fitted to the scaling law and yield values of α as 0.32 and 0.3 (see solid and dashed lines in Figure 5). However the obtained index (α) for viscoplastic drops is slightly higher than the value ($\alpha = 0.25$) of Newtonian cases reported in literature[9]. Similar effect has also been observed for other type (shear-thinning) of non-Newtonian drops[17]. Though the yield stress does inhibit the spreading of liquid lamella to some degree, a monotonous increase of maximum spreading diameter with respect to We is observed for all viscoplastic drops. This is due to the dominance of inertial force during spreading. The considered range of Weber numbers is from 10 to 150, which means inertial force is at least one order of magnitude higher than surface tension. While the yield stress is either smaller than or comparable with surface tension (check B values in Table 1), inertial force always plays a major role in spreading for all cases.

3.3 Maximum bouncing height

The maximum bouncing height (H_{max}) denotes the maximum height reached by the drop centre of mass during rebound. While the maximum spreading diameter indicates how much of the initial impact kinetic energy is stored as surface energy as the drop is deformed, the maximum bouncing height indicates how much energy remains after the impact or, alternatively, can give a measure of the total energy dissipation during impact when subtracted from the impact kinetic energy[17].

The normalised maximum bouncing height (H_{max}/D_0) of drops of model fluids with respect to the equilibrium drop diameter is displayed in Figure 6 as a function of the impact Weber number. The data of drops with a Bingham-Capillary number higher than unity ($B = 1.2$&2.3) are labelled using open symbols while others are represented by filled symbols. For drops with a relatively low yield stress ($B = 0.052, 0.16$&0.52), the rebound behavior is similar to high viscosity Newtonian drops: after an initial almost linear increase with respect to We the maximum bouncing height tends to reach a plateau at high impact Weber numbers[32]. This behaviour is probably due to the fact that the viscous dissipation during impact becomes large enough to compensate the increment in bouncing height, due to the increase of surface energy stored during impact.

When the yield stress force is close to but still slightly lower than surface tension ($B = 0.88$), no sign of plateau is observed in the considered We range except for the linear increase. Nevertheless the rebound behavior of drops with values of B over unity ($B = 1.2$&2.3) is totally different from others: the maximum bouncing height of drop with a yield stress force slightly higher than surface tension ($B = 1.2$) fluctuates between $0.5D_0$ and D_0 whilst that of drop with an even higher Bingham-Capillary number ($B = 2.3$) stays around $0.5D_0$ regardless of the change of impact Weber number. We note that for higher yield stress magnitudes ($B = 1.2$&2.3) drops keep a prolate morphology at impact, therefore the definition of Weber number based on the equivalent equilibrium drop diameter is not as accurate as in other cases. However, even a large correction of the Weber number for these points would not affect the main results; with reference to Figure 6, for example, this would cause a horizontal shift of the points in the two corresponding series (open symbols), which would not change the conclusion either qualitatively or quantitatively.

Figure 6 can be replotted as Figure 7 by replacing the Weber number with the Bingham-Capillary number for x-axis in order to show the effect of B on maximum bouncing height directly. The data are regrouped into five sets according to impact We range. The varying trend of H_{max}/D_0 with respect to B is similar for all We range groups: after an initial plateau at low Bingham-Capillary numbers, the maximum bouncing height drops considerably as B exceeds unity. This is related to the high resistance of yield stress to counter the retraction driven by surface tension, which will be discussed in next paragraph.

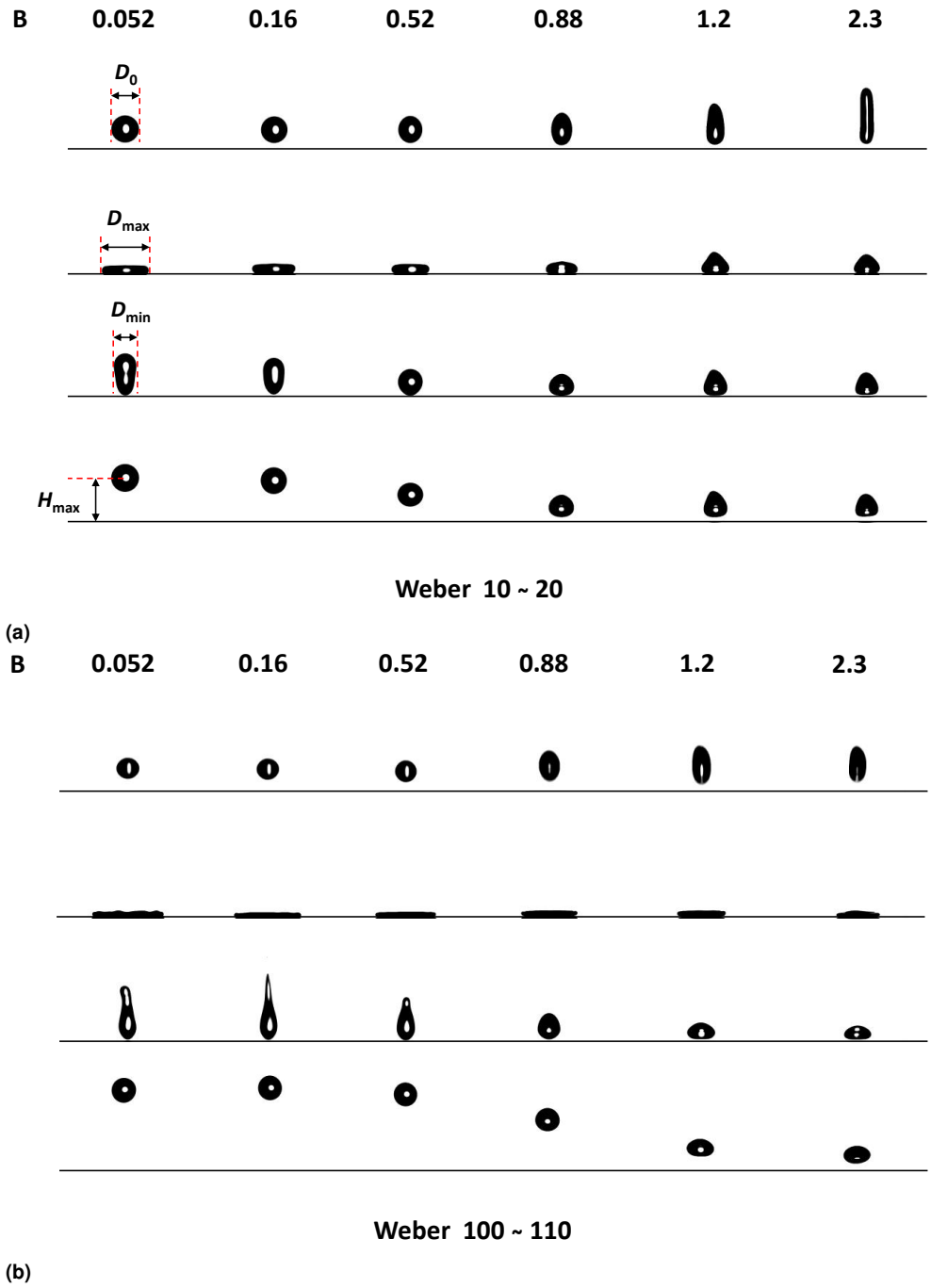

Fig. 4 Impact morphology of Leidenfrost different viscoplastic drops with different Bingham-Capillary numbers: (a) Weber number 10 20; (b) Weber number 100 110. The first row indicates the Bingham-Capillary number of impacting drop, second the beginning of impact, third the maximum spreading, fourth the beginning of bouncing and last the maximum bouncing.

3.4 Minimum retracting diameter

The diameter of the prolate bouncing drop formed at the beginning of rebound is called the 'minimum retracting diameter' (D_{min}). This parameter can qualitatively describe the magnitude of retraction after the spreading phase, in other words, the effect of yield stress to counter the retraction driven by surface tension. Figure 8 shows the normalised minimum retracting diameter (D_{min}/D_0) with respect to the equilibrium drop diameter of the drops of model fluids as a function of the impact Weber number. For cases of low Bingham-Capillary numbers ($B = 0.052, 0.16\&0.52$), the variation of minimum retracting diameter with respect to impact Weber number follows the same pattern: after an initial drop the D_{min}/D_0 reaches a plateau as We increases. In addition, the minimum retracting diameter is always smaller than the equilibrium drop diameter ($D_{min}/D_0 < 1$), which means the surface tension still dominates during the retraction process for low B numbers. However when B increases to 0.88, the value of D_{min} fluctuates around the equilibrium drop diameter

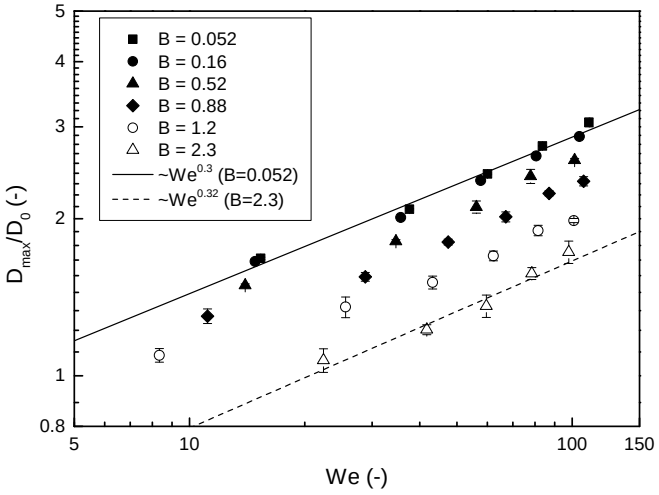

Fig. 5 Maximum spreading diameter of the drops of model fluids as a function of the impact Weber number. Lines represent the fitting results of scaling law for $B = 0.052$ (solid) and $B = 2.3$ (dashed).

($D_{min}/D_0 \approx 1$) indicating that the resistant yield stress is comparable to the surface tension. As the Bingham-Capillary number becomes larger ($B = 2.3$), the minimum retracting diameter even increases monotonously with respect to the Weber number in the considered *We* range. At high impact *We* ($60 \sim 100$), the spreading drop is not able to retract to its equilibrium diameter due to the existence of high yield stress ($D_{min}/D_0 > 1$) and the inertial deformation upon impact becomes permanent, resulting in an oblate bouncing drop (see Figure 4b). Here the ratio of the maximum spreading diameter to the minimum retracting diameter is defined as the 'retraction coefficient' (D_{max}/D_{min}) and its correlation with the maximum bouncing height is plotted in Figure 9a. A linear correlation between these two parameters is obtained:

$$\mathrm{H}_{max}/\mathrm{D}_0 = 1.15(\mathrm{D}_{max}/\mathrm{D}_{min}) - 0.968. \quad (2)$$

This feature indicates that the deformation of the drop during retraction stage is crucial to the bouncing behavior while the assumption that the disk-like drop remains rigid in the so-called disk model (e.g.,[1]) may not be physical. Thus, the major contribution to the rebound of a drop impacting onto a heated surface is the surface tension whilst the contribution of intrinsic elasticity of the vapour cushion between the drop and the surface is negligible. We note that when the same analysis is done on drops of water or dilute polymer solutions (Figure 9b), data do not display a clear linear correlation, except in the lower limit of the bouncing height (Weber number), both because of the lower viscosity, which makes the drop shape highly irregular at the beginning of rebound, and to the more complex energy dissipation mechanism[16–18].

4 Conclusions

The impact morphology of viscoplastic drops onto a heated surface in Leidenfrost regime was studied experimentally though high-speed imaging. Several important parameters which characterize the impact morphology (such as maximum spreading diameter, minimum retracting diameter and maximum bouncing height etc.) were measured by analysing the impact process. Due to the dominance of inertial force during spreading a monotonous increase of maximum spreading diameter with respect to *We* was observed for all viscoplastic drops. For drops with a relatively low yield stress, the rebound behavior is similar to high viscosity Newtonian drops. As the yield stress grows, surface forces are no longer able to minimize the free surface of the drop, and the inertial deformation upon impact becomes permanent. These effects can be interpreted in terms of the Bingham-Capillary number, which compares the yield stress magnitude and the capillary (Laplace) pressure. In addition the linear correlation between retraction coefficient (D_{max}/D_{min}) and maximum bouncing height in the considered *We* range means the deformation of the drop during retraction is crucial to its rebound behavior and the main contribution to drop rebound is due to surface forces, and not

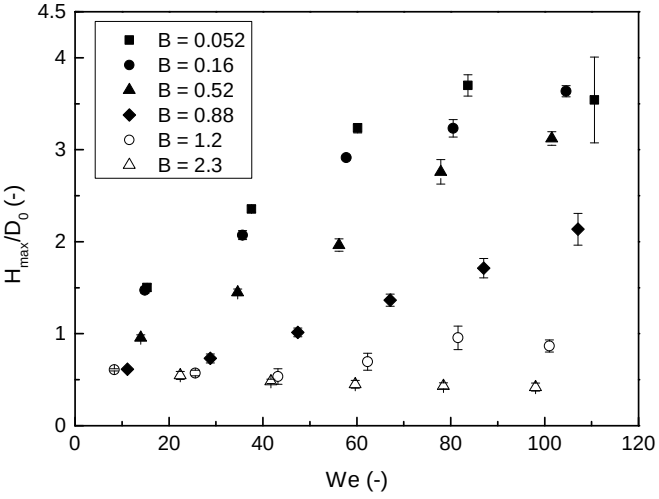

Fig. 6 Maximum bouncing height of the drops of model fluids as a function of the impact Weber number.

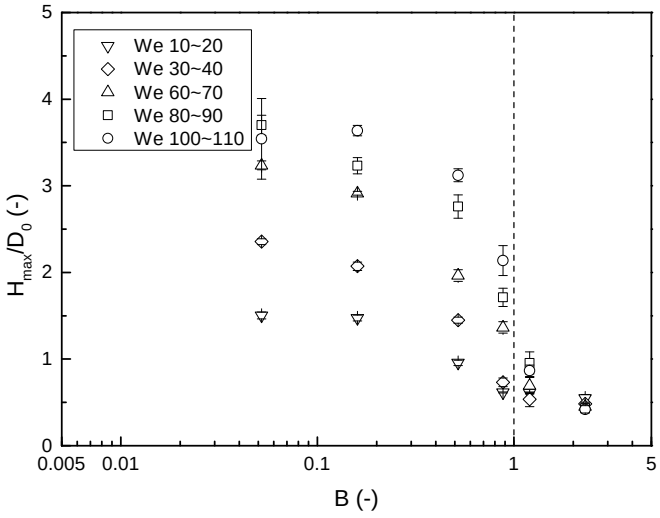

Fig. 7 Maximum bouncing height of the drops of model fluids as a function of the Bingham-Capillary number.

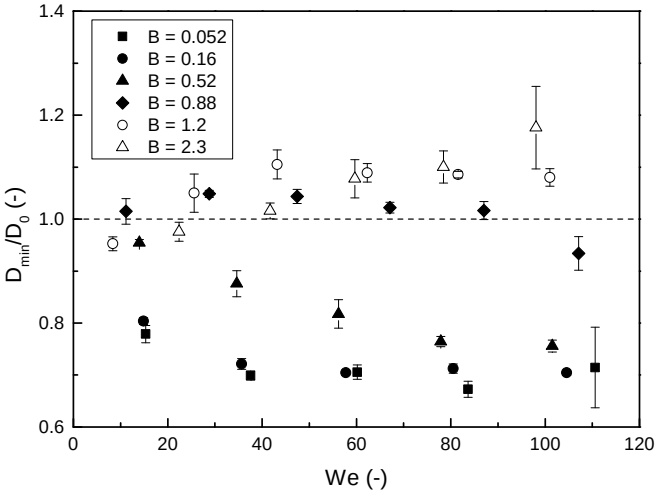

Fig. 8 Minimum retracting diameter of the drops of model fluids as a function of the impact Weber number.

to the intrinsic elasticity of the vapour cushion between the drop and the surface, which is a major assumption in one of the existing models.

References

1 M. Rein, *Drop-Surface Interactions*, Springer Wien New York, 2002.

2 L. Wachters and N. Westerling, *Chemical Engineering Science*, 1966, **21**, 1047–1056.

3 B. Gottfried, C. Lee and K. Bell, *International Journal of heat and mass transfer*, 1966, **9**, 1167–1188.

4 D. Quere, *Annual Review of Fluid Mechanics*, 2013, **45**, 197–215.

5 M. Goldshtik, V. Khanin and V. Ligai, *Journal of Fluid Mechanics*, 1986, **166**, 1–20.

6 J. Snoeijer, P. Brunet and J. Eggers, *Physical Review E*, 2009, **79**, 036307.

7 J. D. Bernardin, C. J. Stebbins and I. Mudawar, *International Journal of Heat and Mass Transfer*, 1997, **40**, 247–267.

8 J. D. Bernardin and I. Mudawar, *Journal of heat transfer*, 2004, **126**, 272–278.

9 A.-L. Biance, F. Chevy, C. Clanet, G. Lagubeau and D. Quéré, *Journal of Fluid Mechanics*, 2006, **554**, 47–66.

10 J. Burton, R. Sharpe, A. van der Veen, A. Franco and S. Nagel, *Physical Review Letters*, 2012, **109**, 074301.

11 A. Moreira, A. Moita and M. Panao, *Progress in energy and combustion science*, 2010, **36**, 554–580.

12 T. Tran, H. Staat, A. Prosperetti, C. Sun and D. Lohse, *Physical Review Letters*, 2012, **108**, 036101.

13 V. Bertola, *International journal of heat and mass transfer*, 2015, **85**, 430–437.

14 V. Bertola, *Experiments in fluids*, 2004, **37**, 653–664.

15 V. Bertola and K. Sefiane, *Physics of Fluids*, 2005, **17**, 108104.

16 V. Bertola, *International journal of heat and mass transfer*, 2009, **52**, 1786–1793.

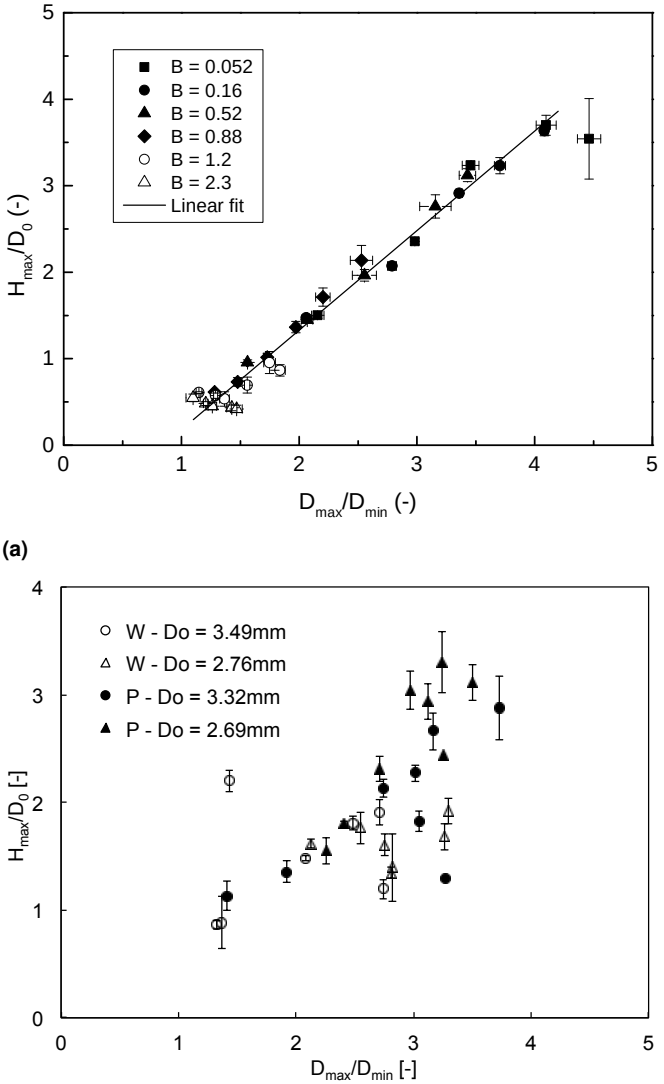

Fig. 9 Maximum bouncing height of the drops of model fluids as a function of the retraction coefficient: (a) viscoplastic drops; (b) water and dilute polymer solution drops of different diameter[16].

17 K. Black and V. Bertola, *Atomization and Sprays*, 2013, **23**, year.

18 V. Bertola, *Experimental Thermal and Fluid Science*, 2014, **52**, 259–269.

19 G. German and V. Bertola, *Physics of Fluids*, 2010, **22**, 033101.

20 G. German and V. Bertola, *Journal of Physics: Condensed Matter*, 2009, **21**, 375111.

21 G. German and V. Bertola, *Colloids and Surfaces A: Physicochemical and Engineering Aspects*, 2010, **366**, 18–26.

22 B. C. Blackwell, M. E. Deetjen, J. E. Gaudio and R. H. Ewoldt, *Physics of Fluids*, 2015, **27**, 043101.

23 M. Jalaal, N. J. Balmforth and B. Stoeber, *Langmuir*, 2015, **31**, 12071–12075.

24 T. Mao, D. Kuhn and H. Tran, *AIChE Journal*, 1997, **43**, 2169–2179.

25 D. Richard and D. Quéré, *EPL (Europhysics Letters)*, 2000, **50**,

769.
26 A. Karl, M. Rieber, M. Schelkle, K. Anders and A. Frohn, *ASME-PUBLICATIONS-FED*, 1996, **236**, 201–206.
27 H. Fujimoto and N. Hatta, *Journal of fluids engineering*, 1996, **118**, 142–149.
28 V. Bertola, *Journal of Physics: Condensed Matter*, 2008, **21**, 035107.
29 S. Curran, R. Hayes, A. Afacan, M. Williams and P. Tanguy, *Journal of food science*, 2002, **67**, 176–180.
30 G. P. Roberts and H. A. Barnes, *Rheologica Acta*, 2001, **40**, 499–503.
31 J. Boujlel and P. Coussot, *Soft Matter*, 2013, **9**, 5898–5908.
32 S. Chen and V. Bertola, *Proc. 26th European Conference on Liquid Atomization and Spray Systems, 8-10 Sep. 2014, Bremen, Germany*, 2014.